Journal of Systems Engineering and Electronics
Vol. 33, No. 1, February 2022, pp.60 – 71

Subspace detection for range-spread target to suppress interference: exploiting persymmetry in non-homogeneous scenario

GAO Yongchan[1], MAO Linlin[2,*], ZHU Shengqi[3], and ZUO Lei[3]

1. Department of Electronic Engineering, Xidian University, Xi'an 710071, China; 2. Institute of Acoustics, Chinese Academy of Sciences, Beijing 100190, China; 3. National Laboratory of Radar Signal Processing, Xidian University, Xi'an 710071, China

Abstract: This paper deals with subspace detection for range-spread target in non-homogeneous clutter with unknown covariance matrix where structured interference is presented in the received data. Through exploiting the persymmetry of the clutter covariance matrix, we propose two adaptive target detectors, which are referred to as persymmetric subspace Rao to suppress interference and persymmetric subspace Wald to suppress interference ("PS-Rao-I" and "PS-Wald-I"), respectively. The persymmetry-based design brings in the advantage of easy implementation for small training sample support. The signal flow analysis of the two detectors shows that the PS-Rao-I rejects interference and integrates signals successively through separated matrix projection, while the PS-Wald-I jointly achieves interference elimination and signal combination via oblique projection. In addition, both detectors are shown to be constant false alarm rate detectors, significantly improving the detection performance with other competing detectors under the condition of limited training.

Keywords: adaptive detection, range-spread target, persymmetric structure, Rao test, Wald test.

DOI: 10.23919/JSEE.2022.000007

1. Introduction

Range-spread target detection, especially with application in large scale targets or high-resolution radar, has been extensively studied in recent years [1–6]. To detect a range-spread target, the clutter covariance matrix is generally not known so that a set of training data free of useful signal is used to estimate it. A common assumption concerning training data is the homogeneous environment, namely, the training data is with the same distribution as the clutter in the cell under test (CUT). However, the homogeneous assumption is difficult to satisfy in practice due to terrain variations and system factors, such as the presence of interference and array configuration. Unlike the homogeneous environment, the partially homogeneous environment (PHE), where both the clutter in CUT and training data share the same covariance matrix up to an unknown power scaling factor, is more robust to power variation between test data and training signals [7–10]. To detect a range-spread target in the PHE, considerable research efforts have been devoted in [11–14].

Apart from the non-homogeneous scenario, the existence of interference caused by electronic countermeasure systems or civil broadcasting system is a key factor affecting the detection performance. It is therefore important to consider interference suppression in the design of detectors. The structured interference modeled by a subspace to describe the multipath effect or uncertainty of direction-of-arrival associated with the interference steering vector, has been intensively investigated in adaptive detection [15–24]. Adaptive detection of a point-like target in the presence of subspace interference for PHE was addressed in [15–16] under the criterion of generalized likelihood ratio test (GLRT) and Wald, and was further investigated within the framework of invariance theory in [17]. When it comes to range-spread targets, the design of GLRT and its two-step variation for partially homogeneous Gaussian noise plus subspace interference was considered in [18], and its relevant Rao detection was provided in [19]. Extensions of [18] to the compound Gaussian environment was made in [20].

A possible solution to decrease the training amount associated with adaptive detectors was reported in [25], by exploiting the persymmetric structure of the disturbance covariance matrix. Thereafter, many detection investigations concerning the persymmetry in the PHE have been developed in [26–31]. Specifically, the authors of [26]

Manuscript received July 16, 2020.
*Corresponding author.
This work was supported by the National Natural Science Foundation of China (61901467; 61701370), the Aeronautical Foundation of China (20180181001), China Postdoctoral Science Foundation (2019M 653561; 2020T130493), the Aerospace Science and Technology Fund (SAST2018-098), and the National Defense Science and Technology Foundation of China (2019-JCJQ-JJ-060).

proposed a persymmetric GLRT resorting to the two-step method, and its corresponding performance assessment was presented in [27]. Persymmetric Rao and persymmetric Wald detectors were established in [28] for point-like targets in the PHE, and was extended to the detection of range-spread targets in [29]. The persymmetric adaptive cosine estimator (ACE) in the PHE was developed in [30]. Meanwhile, adaptive signal detection in PHE and persymmetric Gaussian disturbance was addressed in [31] within the framework of invariance theory. Other examples of persymmetric detectors can be found in [32−45].

The persymmetric GLRT for detecting a range-spread target in structured interference was considered in [46]. It is given that the uniformly most powerful (UMP) test for the detection problem in [46], due to the lack of information on the signal/interference coordinates and the noise covariance matrix. It is therefore of utmost importance to investigate different detectors with various features, among which, Rao and Wald test are most commonly used as an alternative to GLRT with reduced computational complexity and sometimes better performance. As far as we know, no previous work has conducted the adaptive Rao and Wald detection of multi-rank subspace signal in PHE to suppress interference.

In this paper, we adopt Rao and Wald tests for subspace detection of range-spread target embedded in structured interference and non-homogeneous noise. The main contributions are as follows:

(i) In order to relax the restrictions on the number of training signal and ease the computational burden, we devise two persymmetric subspace detectors with the help of unitary transformation, namely the persymmetric subspace Rao detector and the persymmetric subspace Wald detector in the case of subspace interference (referred to as the “PS-Rao-I” and “PS-Wald-I”respectively), which incorporate the persymmetric structure of the disturbance covariance matrix in the design of the detectors.

(ii) Block diagram for the proposed detectors is presented to demonstrate the signal flow of each detector. Specifically, the PS-Rao-I projects the transformed signal into the orthogonal complement of the interference subspace and the signal subspace successively, which leads to separated interference rejection and signal integration process. The PS-Wald-I, in contrast, projects the transformed signal into the signal subspace along the interference subspace via oblique projection, which achieves interference elimination and signal combination simultaneously. Theoretical derivation shows that the two detectors exhibit constant false alarm rate (CFAR) property with respect to (w.r.t.) the unknown covariance matrix and the power scaling factor.

(iii) Numerical examples based on both simulated data and real radar data are presented to demonstrate the effectivity and efficiency of the proposed methods.

The remainder of this paper is organized as follows. Section 2 presents the data model. Section 3 contains the derivation and discussion of the proposed tests. Numerical examples and experimental results are provided in Section 4. The concluding remarks are summarized in Section 5.

2. Problem statement

Consider a linear array with N uniformly-spaced sensors receiving the echo signals reflected from a range-spread target in PHE. Our task is to decide whether the target which occupies L successive range cells, presents or not in the range bin under test. Denote by $\boldsymbol{x}_l \in \mathbb{C}^N$, $l = 1,2,\cdots,L$ the data collected from the lth range bin. The detection problem can be formulated in terms of a binary hypothesis test.

Under hypothesis H_1, $\boldsymbol{x}_l$ contains signal $\boldsymbol{s}_l$, interference $\boldsymbol{i}_l$ and noise $\boldsymbol{n}_l$. The signal and the interference are supposed to lie in two independent subspaces $\mathrm{Sp}(\boldsymbol{H})$ and $\mathrm{Sp}(\boldsymbol{G})$ spanned by full-column-rank matrices $\boldsymbol{H} = [\boldsymbol{h}_1, \boldsymbol{h}_2, \cdots, \boldsymbol{h}_r] \in \mathbb{C}^{N\times r}$ and $\boldsymbol{G} = [\boldsymbol{g}_1, \boldsymbol{g}_2, \cdots, \boldsymbol{g}_s] \in \mathbb{C}^{N\times s}$, respectively, i.e., $\boldsymbol{s}_l = \boldsymbol{H}\boldsymbol{\beta}_l$ and $\boldsymbol{i}_l = \boldsymbol{G}\boldsymbol{q}_l$, with $\boldsymbol{\beta}_l \in \mathbb{C}^r$ and $\boldsymbol{q}_l \in \mathbb{C}^s$ being the unknown coordinates. By contrast, under the null hypothesis H_0, $\boldsymbol{x}_l = \boldsymbol{i}_l + \boldsymbol{n}_l$.

In addition to the signal under test, we assume that a signal-free training data set $\boldsymbol{x}_{n,k} \in \mathbb{C}^N$ $(k = 1,2,\cdots,K)$ that does not contain the signal to be detected can be collected from adjacent range units. That is, $\boldsymbol{x}_{n,k} = n_{n,k}$ with $\boldsymbol{n}_{n,k}$ denoting the noise component in the training set which shares the same covariance structure as $\boldsymbol{n}_l$. Assume that $\boldsymbol{n}_{n,k}$ are independently identically distributed (i.i.d) Gaussian random vectors with zero mean and unknown covariance matrix $\boldsymbol{\Delta}$. $\boldsymbol{n}_l$ is modeled similarly but with covariance matrix $\gamma\boldsymbol{\Delta}$, where $\gamma > 0$ stands for an unknown deterministic parameter, which determines the statistical characteristic of the PHE.

The problem of interest at hand can be formulated as the hypothesis test below:

$$\begin{cases} \mathrm{H}_0 : \boldsymbol{X} = \boldsymbol{G}\boldsymbol{Q} + \boldsymbol{N}, \boldsymbol{X}_K = \boldsymbol{N}_K \\ \mathrm{H}_1 : \boldsymbol{X} = \boldsymbol{H}\boldsymbol{B} + \boldsymbol{G}\boldsymbol{Q} + \boldsymbol{N}, \boldsymbol{X}_K = \boldsymbol{N}_K \end{cases} \tag{1}$$

where

$$\boldsymbol{X} = [\boldsymbol{x}_1, \boldsymbol{x}_2, \cdots, \boldsymbol{x}_L] \in \mathbb{C}^{N\times L}, \tag{2}$$

$$\boldsymbol{N} = [\boldsymbol{n}_1, \boldsymbol{n}_2, \cdots, \boldsymbol{n}_L] \in \mathbb{C}^{N\times L}, \tag{3}$$

$$\boldsymbol{X}_K = [\boldsymbol{x}_{n,1}, \boldsymbol{x}_{n,2}, \cdots, \boldsymbol{x}_{n,K}] \in \mathbb{C}^{N\times K}, \tag{4}$$

$$\boldsymbol{N}_K = [\boldsymbol{n}_{n,1}, \boldsymbol{n}_{n,2}, \cdots, \boldsymbol{n}_{n,K}] \in \mathbb{C}^{N\times K}, \tag{5}$$

$$\boldsymbol{B}=[\boldsymbol{\beta}_1,\boldsymbol{\beta}_2,\cdots,\boldsymbol{\beta}_L]\in\mathbb{C}^{r\times L}, \tag{6}$$

and

$$\boldsymbol{Q}=[\boldsymbol{q}_1,\boldsymbol{q}_2,\cdots,\boldsymbol{q}_L]\in\mathbb{C}^{s\times L}. \tag{7}$$

Considering the spatial structure of the uniform linear array, $\boldsymbol{h}_i(i=1,2,\cdots,r)$ and $\boldsymbol{g}_i(i=1,2,\cdots,s)$ satisfy a persymmetric property, i.e., $\boldsymbol{h}_i=\boldsymbol{J}_N\boldsymbol{h}_i^*$ and $\boldsymbol{g}_i=\boldsymbol{J}_N\boldsymbol{g}_i^*$, where $\boldsymbol{J}_N\in\mathbb{C}^N$ stands for the exchange matrix with the unit elements residing on the counter diagonal and all other elements being zero, and * denotes the conjugate operator. It is straightforward to show that the covariance matrix $\boldsymbol{\Delta}$ is persymmetric, which can be defined as follows:

$$\boldsymbol{\Delta}=\boldsymbol{J}_N\boldsymbol{\Delta}^*\boldsymbol{J}_N. \tag{8}$$

According to the persymmetric property, we can construct a unitary matrix to transform complex matrix $\boldsymbol{\Delta}$ to a real one. Such a unitary matrix is given by [26]

$$\boldsymbol{T}=\begin{cases}\dfrac{1}{\sqrt{2}}\begin{bmatrix}\boldsymbol{I}_{N/2} & \boldsymbol{J}_{N/2}\\ \mathrm{j}\boldsymbol{I}_{N/2} & -\mathrm{j}\boldsymbol{J}_{N/2}\end{bmatrix}, & N \text{ is even}\\ \dfrac{1}{\sqrt{2}}\begin{bmatrix}\boldsymbol{I}_{(N-1)/2} & 0 & \boldsymbol{J}_{(N-1)/2}\\ 0 & \sqrt{2} & 0\\ \mathrm{j}\boldsymbol{I}_{(N-1)/2} & 0 & -\mathrm{j}\boldsymbol{J}_{(N-1)/2}\end{bmatrix}, & N \text{ is odd}\end{cases} \tag{9}$$

with $\boldsymbol{I}_n$ being the n-dimensional identity matrix. By exploiting the transformation matrix $\boldsymbol{T}$ to the data under test, we can readily express the problem of interest as

$$\begin{cases}\mathrm{H}_0: \boldsymbol{Y}=\boldsymbol{G}_p\boldsymbol{Q}+\boldsymbol{N}_p, \boldsymbol{Y}_K=\boldsymbol{N}_{pK}\\ \mathrm{H}_1: \boldsymbol{Y}=\boldsymbol{H}_p\boldsymbol{B}+\boldsymbol{G}_p\boldsymbol{Q}+\boldsymbol{N}_p, \boldsymbol{Y}_K=\boldsymbol{N}_{pK}\end{cases}. \tag{10}$$

Recall that both $\boldsymbol{n}_{n,k}$ and $\boldsymbol{n}_l$ are i.i.d Gaussian random vectors with zero mean, they follow the properties of persymmetric Hermitian matrices that $\boldsymbol{N}_p\sim\mathrm{CN}(\boldsymbol{0},\gamma\boldsymbol{R})$ and $\boldsymbol{N}_{pK}\sim\mathrm{CN}(\boldsymbol{0},\boldsymbol{R})$ where

$$\boldsymbol{R}=\boldsymbol{T}\boldsymbol{\Delta}\boldsymbol{T}^{\mathrm{H}} \tag{11}$$

represents a real symmetric matrix, and $(\cdot)^{\mathrm{H}}$ denotes conjugate transpose. From a practical view, we know that $\boldsymbol{R}$ is unavailable, and we can get its maximum likelihood estimation (MLE) by

$$\widehat{\boldsymbol{R}}_p=\Re\left(\frac{1}{K}\sum_{k=1}^{K}\boldsymbol{y}_k\boldsymbol{y}_k^{\mathrm{H}}\right) \tag{12}$$

where $\Re(\cdot)$ denotes the real part of a matrix, and $\boldsymbol{y}_k$ is the kth column of $\boldsymbol{Y}_K$.

3. Persymmetric Rao and Wald detector in subspace interference

We now consider the target detection problem in the presence of subspace interference in the PHE, and develop the corresponding PS-Rao-I and PS-Wald-I detector.

3.1 PS-Rao-I detector design

First, we denote $\boldsymbol{\Theta}$ the parameter vector given by

$$\boldsymbol{\Theta}=[\boldsymbol{\Theta}_r^{\mathrm{T}},\boldsymbol{\Theta}_s^{\mathrm{T}}]^{\mathrm{T}}, \tag{13}$$

where $\boldsymbol{\Theta}_r=\mathrm{vec}(\boldsymbol{B})$ and $\boldsymbol{\Theta}_s=[\gamma,\mathrm{vec}^{\mathrm{T}}(\boldsymbol{Q}), \ \mathrm{vec}^{\mathrm{T}}(\boldsymbol{R})]$ are called by the interesting parameter and nuisance parameter, with $\mathrm{vec}(\cdot)$ being the vectorization operation.

According to [47], we can construct the Rao detection as

$$t_{\mathrm{Rao}}=\left.\frac{\partial\ln f_1}{\partial\boldsymbol{\Theta}_r}\right|^{\mathrm{T}}_{\boldsymbol{\Theta}=\widehat{\boldsymbol{\Theta}}_0}[\boldsymbol{I}^{-1}(\widehat{\boldsymbol{\Theta}}_0)]_{\boldsymbol{\Theta}_r\boldsymbol{\Theta}_r}\left.\frac{\partial\ln f_1}{\partial\boldsymbol{\Theta}_r^*}\right|_{\boldsymbol{\Theta}=\widehat{\boldsymbol{\Theta}}_0} \tag{14}$$

where $\widehat{\boldsymbol{\Theta}}_0$ is the MLE of $\boldsymbol{\Theta}$ under H_0. f_1 represents the joint probability density functions (PDF) of $\boldsymbol{Y}$ and $\boldsymbol{Y}_K$ under H_1 given by

$$f_1(\boldsymbol{Y},\boldsymbol{Y}_K)=\frac{\exp\{-\mathrm{tr}(\boldsymbol{R}^{-1}\boldsymbol{Z}\boldsymbol{Z}^{\mathrm{H}}/\gamma)-\mathrm{tr}(\boldsymbol{R}^{-1}\boldsymbol{M})\}}{\pi^{N(K+L)}\gamma^{NL}\det(\boldsymbol{R})^{K+L}} \tag{15}$$

where $\boldsymbol{Z}\triangleq\boldsymbol{Y}-\boldsymbol{S}_p\boldsymbol{A},\boldsymbol{S}_p\triangleq[\boldsymbol{H}_p,\boldsymbol{G}_p],\boldsymbol{A}\triangleq[\boldsymbol{B}^{\mathrm{H}},\boldsymbol{Q}^{\mathrm{H}}]^{\mathrm{H}}$, and $\boldsymbol{M}=\boldsymbol{Y}_K\boldsymbol{Y}_K^{\mathrm{H}}$ is the sample covariance matrix. Then, denote by $\boldsymbol{I}(\boldsymbol{\Theta})$ the Fisher information matrix that can be described as

$$\boldsymbol{I}(\boldsymbol{\Theta})=\mathrm{E}\left\{\left[\frac{\partial\ln f_1(\boldsymbol{Y})}{\partial\boldsymbol{\Theta}^*}\right]\left[\frac{\partial\ln f_1(\boldsymbol{Y})}{\partial\boldsymbol{\Theta}^{\mathrm{T}}}\right]\right\}. \tag{16}$$

Taking the derivative of the logarithm of (15) with respect to $\boldsymbol{B}$ and $\boldsymbol{B}^*$ leads to

$$\frac{\partial\ln f_1(\boldsymbol{Y},\boldsymbol{Y}_K)}{\partial\mathrm{vec}(\boldsymbol{B})}=\mathrm{vec}(\boldsymbol{Z}^{\mathrm{H}}\boldsymbol{R}^{-1}\boldsymbol{H}_p)^{\mathrm{T}}/\gamma, \tag{17}$$

and

$$\frac{\partial\ln f_1(\boldsymbol{Y},\boldsymbol{Y}_K)}{\partial\mathrm{vec}(\boldsymbol{B}^*)}=\mathrm{vec}(\boldsymbol{H}_p^{\mathrm{H}}\boldsymbol{R}^{-1}\boldsymbol{Z})/\gamma. \tag{18}$$

Note that $\boldsymbol{I}(\boldsymbol{\Theta})$ can be generally partitioned as

$$\boldsymbol{I}(\boldsymbol{\Theta})=\begin{bmatrix}\boldsymbol{I}_{\boldsymbol{\Theta}_r\boldsymbol{\Theta}_r}(\boldsymbol{\Theta}) & \boldsymbol{I}_{\boldsymbol{\Theta}_r\boldsymbol{\Theta}_s}(\boldsymbol{\Theta})\\ \boldsymbol{I}_{\boldsymbol{\Theta}_s\boldsymbol{\Theta}_r}(\boldsymbol{\Theta}) & \boldsymbol{I}_{\boldsymbol{\Theta}_s\boldsymbol{\Theta}_s}(\boldsymbol{\Theta})\end{bmatrix}. \tag{19}$$

Substituting (17) and (18), into (16), yields,

$$\begin{gathered}\boldsymbol{I}_{\boldsymbol{\Theta}_r\boldsymbol{\Theta}_r}(\boldsymbol{\Theta})=\mathrm{E}[\mathrm{vec}(\boldsymbol{H}_p^{\mathrm{H}}\boldsymbol{R}^{-1}\boldsymbol{Z}/\gamma)\mathrm{vec}^{\mathrm{T}}(\boldsymbol{H}_p^{\mathrm{T}}\boldsymbol{R}^{-\mathrm{T}}\boldsymbol{Z}^*/\gamma)]=\\ \mathrm{E}\{(\boldsymbol{I}_L\otimes\boldsymbol{H}_p^{\mathrm{H}}\boldsymbol{R}^{-1})\mathrm{vec}(\boldsymbol{Z})\cdot[(\boldsymbol{I}_L\otimes\boldsymbol{H}_p^{\mathrm{T}}\boldsymbol{R}^{-\mathrm{T}})\mathrm{vec}(\boldsymbol{Z}^*)]^{\mathrm{T}}\}/\gamma^2=\\ (\boldsymbol{I}_L\otimes\boldsymbol{H}_n^{\mathrm{H}}\boldsymbol{R}^{-1}\boldsymbol{H}_p)/\gamma.\end{gathered} \tag{20}$$

Likewise, it is straightforward to verify that $\boldsymbol{I}_{\boldsymbol{\Theta}_r\boldsymbol{\Theta}_s}(\boldsymbol{\Theta})$ is a null matrix, which then results in

$$[\boldsymbol{I}^{-1}(\boldsymbol{\Theta})]_{\boldsymbol{\Theta}_r\boldsymbol{\Theta}_r}=\boldsymbol{I}^{-1}_{\boldsymbol{\Theta}_r\boldsymbol{\Theta}_r}=\gamma(\boldsymbol{I}_L\otimes\boldsymbol{H}_p^{\mathrm{H}}\boldsymbol{R}^{-1}\boldsymbol{H}_p)^{-1}. \tag{21}$$

Inserting (17), (18) and (21) into (14), and setting $\boldsymbol{B}=\boldsymbol{0}_{r\times L}$ leads to the PS-Rao-I test for given γ, $\boldsymbol{Q}$ and $\boldsymbol{R}$,

$$\begin{gathered}t_{\text{PS-Rao-I}}=\mathrm{vec}^{\mathrm{T}}\left[(\boldsymbol{Y}-\boldsymbol{G}_p\boldsymbol{Q})^{\mathrm{H}}\boldsymbol{R}^{-1}\boldsymbol{H}_p\right]^{\mathrm{T}}\cdot\\ \left[\boldsymbol{I}_L\otimes(\boldsymbol{H}_p^{\mathrm{H}}\boldsymbol{R}^{-1}\boldsymbol{H}_p)^{-1}\right]\cdot\mathrm{vec}\left[(\boldsymbol{H}_p^{\mathrm{H}}\boldsymbol{R}^{-1}(\boldsymbol{Y}-\boldsymbol{G}_p\boldsymbol{Q})\right]/\gamma=\\ \mathrm{tr}[(\boldsymbol{Y}-\boldsymbol{G}_p\boldsymbol{Q})^{\mathrm{H}}\boldsymbol{R}^{-1}\boldsymbol{H}_p(\boldsymbol{H}_p^{\mathrm{H}}\boldsymbol{R}^{-1}\boldsymbol{H}_p)^{-1}\cdot\end{gathered}$$

$$\boldsymbol{H}_p^{\mathrm{H}}\boldsymbol{R}^{-1}(\boldsymbol{Y}-\boldsymbol{G}_p\boldsymbol{Q})]/\gamma \tag{22}$$

where $\mathrm{tr}(\cdot)$ denotes the trace of a matrix.

Next, we need to estimate $\boldsymbol{Q}$ in (22). By taking the derivative of the logarithm of (15) with $\boldsymbol{B}=\boldsymbol{0}_{r\times L}$ with respect to $\boldsymbol{Q}$, we have, for given $\boldsymbol{R}$, the estimate of $\boldsymbol{Q}$

$$\widehat{\boldsymbol{Q}}=(\overline{\boldsymbol{G}}_p^{\mathrm{H}}\overline{\boldsymbol{G}}_p)^{-1}\overline{\boldsymbol{G}}_p^{\mathrm{H}}\overline{\boldsymbol{Y}} \tag{23}$$

where $\overline{\boldsymbol{G}}_p=\boldsymbol{R}^{-1/2}\boldsymbol{G}_p$ and $\overline{\boldsymbol{Y}}=\boldsymbol{R}^{-1/2}\boldsymbol{Y}$.

Inserting (23) into (22) outputs the PS-Rao-I test for given γ and $\boldsymbol{R}$

$$t_{\text{PS - Rao - I}}=\mathrm{tr}\left(\overline{\boldsymbol{Y}}^{\mathrm{H}}\boldsymbol{P}_{\overline{\boldsymbol{G}}_p}^{\perp}\boldsymbol{P}_{\overline{\boldsymbol{H}}_p}\boldsymbol{P}_{\overline{\boldsymbol{G}}_p}^{\perp}\overline{\boldsymbol{Y}}\right)/\gamma \tag{24}$$

where $\overline{\boldsymbol{H}}_p=\boldsymbol{R}^{-1/2}\boldsymbol{H}_p$.

Substituting $\widehat{\boldsymbol{Q}}$ into (15) with $\boldsymbol{B}=\boldsymbol{0}_{r\times L}$ and ignoring the PDF of $\boldsymbol{Y}_K$ yields

$$f_1(\boldsymbol{Y},\boldsymbol{Y}_K)=\frac{\exp\left\{-\mathrm{tr}\left[\boldsymbol{R}^{-1}(\boldsymbol{Y}-\boldsymbol{G}_p\widehat{\boldsymbol{Q}})(\boldsymbol{Y}-\boldsymbol{G}_p\widehat{\boldsymbol{Q}})^{\mathrm{H}}/\gamma\right]\right\}}{\pi^{\mathrm{NL}}\gamma^{\mathrm{NL}}\det(\boldsymbol{R})^L}=\frac{\exp\left\{-\mathrm{tr}(\overline{\boldsymbol{Y}}^{H}\boldsymbol{P}_{\overline{\boldsymbol{G}}_p}^{\perp}\overline{\boldsymbol{Y}})\right\}}{\pi^{\mathrm{NL}}\gamma^{\mathrm{NL}}\det(\boldsymbol{R})^L}. \tag{25}$$

By taking the derivative of the logarithm of (25) with respect to γ and equating it to zeros results in the MLE of γ for given $\boldsymbol{R}$ under H_0 as

$$\hat{\gamma}_0=\mathrm{tr}(\overline{\boldsymbol{Y}}^{\mathrm{H}}\boldsymbol{P}_{\overline{\boldsymbol{G}}_p}^{\perp}\overline{\boldsymbol{Y}})/\mathrm{NL}. \tag{26}$$

Inserting (26) into (24) and neglecting the constant items leads to the PS-Rao-I test for given $\boldsymbol{R}$:

$$t_{\text{PS - Rao - I}}=\frac{\mathrm{tr}(\overline{\boldsymbol{Y}}^{\mathrm{H}}\boldsymbol{P}_{\overline{\boldsymbol{G}}_p}^{\perp}\boldsymbol{P}_{\overline{\boldsymbol{H}}_p}\boldsymbol{P}_{\overline{\boldsymbol{G}}_p}^{\perp}\overline{\boldsymbol{Y}})}{\mathrm{tr}(\overline{\boldsymbol{Y}}^{\mathrm{H}}\boldsymbol{P}_{\overline{\boldsymbol{G}}_p}^{\perp}\overline{\boldsymbol{Y}})}. \tag{27}$$

Replacing $\boldsymbol{R}$ with the MLE according to (12), we have the persymmetric Rao detector in subspace interference

$$t_{\text{PS - Rao - I}}=\frac{\mathrm{tr}(\widetilde{\boldsymbol{Y}}^{\mathrm{H}}\boldsymbol{P}_{\widetilde{\boldsymbol{G}}_p}^{\perp}\boldsymbol{P}_{\widetilde{\boldsymbol{H}}_p}\boldsymbol{P}_{\widetilde{\boldsymbol{G}}_p}^{\perp}\widetilde{\boldsymbol{Y}})}{\mathrm{tr}(\widetilde{\boldsymbol{Y}}^{\mathrm{H}}\boldsymbol{P}_{\widetilde{\boldsymbol{G}}_p}^{\perp}\widetilde{\boldsymbol{Y}})}=\frac{\|\boldsymbol{P}_{\widetilde{\boldsymbol{H}}_p}\boldsymbol{P}_{\widetilde{\boldsymbol{G}}_p}^{\perp}\widetilde{\boldsymbol{Y}}\|_{\mathrm{F}}^2}{\|\boldsymbol{P}_{\widetilde{\boldsymbol{G}}_p}^{\perp}\widetilde{\boldsymbol{Y}}\|_{\mathrm{F}}^2} \tag{28}$$

where $\widetilde{\boldsymbol{G}}_p=\widehat{\boldsymbol{R}}_p^{-1/2}\boldsymbol{G}_p$, $\widetilde{\boldsymbol{H}}_p=\widehat{\boldsymbol{R}}_p^{-1/2}\boldsymbol{H}$, $\overline{\boldsymbol{Y}}=\widehat{\boldsymbol{R}}_p^{-1/2}\boldsymbol{Y}$, and $\|\cdot\|_{\mathrm{F}}$ denotes the Frobenius norm.

3.2 PS-Wald-I detector design

We now consider the Wald test for the detection problem described in (10). According to [48], we can express the Wald test as

$$t_{\mathrm{Wald}}=(\widehat{\boldsymbol{\Theta}}_{r_1}-\boldsymbol{\Theta}_{r_0})^{\mathrm{H}}\{[\boldsymbol{I}^{-1}(\widehat{\boldsymbol{\Theta}}_1)]_{\boldsymbol{\Theta}_r,\boldsymbol{\Theta}_r}\}^{-1}(\widehat{\boldsymbol{\Theta}}_{r_1}-\boldsymbol{\Theta}_{r_0}) \tag{29}$$

where $\widehat{\boldsymbol{\Theta}}_{r_1}$ denotes the MLE of $\boldsymbol{\Theta}_{r_1}$ under hypothesis H_1, $\boldsymbol{\Theta}_{r_0}$ is the value of $\boldsymbol{\Theta}_{r_1}$ under H_0, and $\{[\boldsymbol{I}^{-1}(\widehat{\boldsymbol{\Theta}}_1)]_{\boldsymbol{\Theta}_r,\boldsymbol{\Theta}_r}\}^{-1}$ stands for the Schur complement of $\boldsymbol{I}_{\boldsymbol{\Theta}_s,\boldsymbol{\Theta}_s}$ evaluated at $\widehat{\boldsymbol{\Theta}}_1$.

To derive the PS-Wald-I test, we need the MLE of $\boldsymbol{B}$ and γ. To obtain the MLE of $\boldsymbol{B}$, we start by deriving the MLE of $\boldsymbol{A}$, which can be obtained by nulling the derivative of $\ln f_1(\boldsymbol{Y})$ with respect to $\boldsymbol{A}$, for given $\boldsymbol{R}$:

$$\widehat{\boldsymbol{A}}=(\boldsymbol{S}_p^{\mathrm{H}}\boldsymbol{R}^{-1}\boldsymbol{S}_p)^{-1}\boldsymbol{S}_p^{\mathrm{H}}\boldsymbol{R}^{-1}\boldsymbol{Y}. \tag{30}$$

Define

$$\boldsymbol{C}\triangleq(\boldsymbol{S}_p^{\mathrm{H}}\boldsymbol{R}^{-1}\boldsymbol{S}_p)^{-1}=\begin{bmatrix}\boldsymbol{C}_{11} & \boldsymbol{C}_{12}\\ \boldsymbol{C}_{21} & \boldsymbol{C}_{22}\end{bmatrix}. \tag{31}$$

Given that

$$\boldsymbol{S}_p^{\mathrm{H}}\boldsymbol{R}^{-1}\boldsymbol{S}_p=\begin{bmatrix}\boldsymbol{H}_p^{\mathrm{H}}\boldsymbol{R}^{-1}\boldsymbol{H}_p & \boldsymbol{H}_p^{\mathrm{H}}\boldsymbol{R}^{-1}\boldsymbol{G}_p\\ \boldsymbol{G}_p^{\mathrm{H}}\boldsymbol{R}^{-1}\boldsymbol{H}_p & \boldsymbol{G}_p^{\mathrm{H}}\boldsymbol{R}^{-1}\boldsymbol{G}_p\end{bmatrix}. \tag{32}$$

According to the theorem about the inverse of a partitioned matrix, we have

$$\boldsymbol{C}_{11}^{-1}=\boldsymbol{H}_p^{\mathrm{H}}\boldsymbol{R}^{-1}\boldsymbol{H}_p-\boldsymbol{H}_p^{\mathrm{H}}\boldsymbol{R}^{-1}\boldsymbol{G}_p(\boldsymbol{G}_p^{\mathrm{H}}\boldsymbol{R}^{-1}\boldsymbol{G}_p)^{-1}\boldsymbol{G}_p^{\mathrm{H}}\boldsymbol{R}^{-1}\boldsymbol{H}_p, \tag{33}$$

and

$$\boldsymbol{C}_{12}=-\boldsymbol{C}_{11}\boldsymbol{H}_p^{\mathrm{H}}\boldsymbol{R}^{-1}\boldsymbol{G}_p(\boldsymbol{G}_p^{\mathrm{H}}\boldsymbol{R}^{-1}\boldsymbol{G}_p)^{-1}. \tag{34}$$

As a result,

$$\widehat{\boldsymbol{B}}=\boldsymbol{C}_{11}\boldsymbol{H}_p^{\mathrm{H}}\boldsymbol{R}^{-1}\boldsymbol{Y}+\boldsymbol{C}_{12}\boldsymbol{G}_p^{\mathrm{H}}\boldsymbol{R}^{-1}\boldsymbol{Y}=\boldsymbol{C}_{11}[\boldsymbol{H}_p^{\mathrm{H}}\boldsymbol{R}^{-1}\boldsymbol{Y}-\boldsymbol{H}_p^{\mathrm{H}}\boldsymbol{R}^{-1}\boldsymbol{G}_p(\boldsymbol{G}_p^{\mathrm{H}}\boldsymbol{R}^{-1}\boldsymbol{G}_p)^{-1}\boldsymbol{G}_p^{\mathrm{H}}\boldsymbol{R}^{-1}\boldsymbol{Y}]=(\overline{\boldsymbol{H}}_p^{\mathrm{H}}\boldsymbol{P}_{\overline{\boldsymbol{G}}_p}^{\perp}\overline{\boldsymbol{H}}_p)^{-1}\overline{\boldsymbol{H}}_p^{\mathrm{H}}\boldsymbol{P}_{\overline{\boldsymbol{G}}_p}^{\perp}\overline{\boldsymbol{Y}}. \tag{35}$$

Substituting (21) and (35) into (29) outputs the PS-Wald-I test, which can be represented as

$$\begin{aligned}t_{\mathrm{Wald}}={}&\mathrm{vec}^{\mathrm{H}}((\overline{\boldsymbol{H}}_p^{\mathrm{H}}\boldsymbol{P}_{\overline{\boldsymbol{G}}_p}^{\perp}\overline{\boldsymbol{H}}_p)^{-1}\overline{\boldsymbol{H}}_p^{\mathrm{H}}\boldsymbol{P}_{\overline{\boldsymbol{G}}_p}^{\perp}\overline{\boldsymbol{Y}})\cdot\\&(\boldsymbol{I}_L\otimes\boldsymbol{H}_p^{\mathrm{H}}\boldsymbol{R}^{-1}\boldsymbol{H}_p)\mathrm{vec}((\overline{\boldsymbol{H}}_p^{\mathrm{H}}\boldsymbol{P}_{\overline{\boldsymbol{G}}_p}^{\perp}\overline{\boldsymbol{H}}_p)^{-1}\overline{\boldsymbol{H}}_p^{\mathrm{H}}\boldsymbol{P}_{\overline{\boldsymbol{G}}_p}^{\perp}\overline{\boldsymbol{Y}})/\gamma=\\&\mathrm{tr}(\overline{\boldsymbol{Y}}^{\mathrm{H}}\boldsymbol{P}_{\overline{\boldsymbol{G}}_p}^{\perp}\overline{\boldsymbol{H}}_p(\overline{\boldsymbol{H}}_p^{\mathrm{H}}\boldsymbol{P}_{\overline{\boldsymbol{G}}_p}^{\perp}\overline{\boldsymbol{H}}_p)^{-1}\overline{\boldsymbol{H}}_p^{\mathrm{H}}\overline{\boldsymbol{H}}_p\cdot\\&(\overline{\boldsymbol{H}}_p^{\mathrm{H}}\boldsymbol{P}_{\overline{\boldsymbol{G}}_p}^{\perp}\overline{\boldsymbol{H}}_p)^{-1}\overline{\boldsymbol{H}}_p^{\mathrm{H}}\boldsymbol{P}_{\overline{\boldsymbol{G}}_p}^{\perp}\overline{\boldsymbol{Y}})/\gamma=\\&\mathrm{tr}(\overline{\boldsymbol{Y}}^{\mathrm{H}}\boldsymbol{P}_{\overline{\boldsymbol{H}}_p|\overline{\boldsymbol{G}}_p}^{\mathrm{H}}\boldsymbol{P}_{\overline{\boldsymbol{H}}_p|\overline{\boldsymbol{G}}_p}\overline{\boldsymbol{Y}})/\gamma\end{aligned} \tag{36}$$

where

$$\boldsymbol{P}_{\overline{\boldsymbol{H}}_p|\overline{\boldsymbol{G}}_p}=\overline{\boldsymbol{H}}_p(\overline{\boldsymbol{H}}_p^{\mathrm{H}}\boldsymbol{P}_{\overline{\boldsymbol{G}}_p}^{\perp}\overline{\boldsymbol{H}}_p)^{-1}\overline{\boldsymbol{H}}_p^{\mathrm{H}}\boldsymbol{P}_{\overline{\boldsymbol{G}}_p}^{\perp} \tag{37}$$

is the oblique projection matrix onto the subspace $\mathrm{Sp}(\overline{\boldsymbol{H}}_p)$ along the subspace $\mathrm{Sp}(\overline{\boldsymbol{G}}_p)$.

Substituting $\widehat{\boldsymbol{A}}$ into (15), and nulling its derivative with respect to γ result in the MLE of γ for given $\boldsymbol{R}$ under H_1 as

$$\hat{\gamma}_1=\mathrm{tr}(\overline{\boldsymbol{Y}}^{\mathrm{H}}\boldsymbol{P}_{\overline{\boldsymbol{S}}_p}^{\perp}\overline{\boldsymbol{Y}})/NL \tag{38}$$

where $\overline{\boldsymbol{S}}_p=\boldsymbol{R}^{-1/2}\boldsymbol{S}_p$, $\boldsymbol{P}_{\overline{\boldsymbol{S}}_p}^{\perp}=\boldsymbol{I}_N-\boldsymbol{P}_{\overline{\boldsymbol{S}}_p}$, and

$$\boldsymbol{P}_{\overline{\boldsymbol{S}}_p}=\boldsymbol{P}_{\overline{\boldsymbol{H}}_p|\overline{\boldsymbol{G}}_p}+\boldsymbol{P}_{\overline{\boldsymbol{G}}_p|\overline{\boldsymbol{H}}_p}. \tag{39}$$

Replacing $\boldsymbol{R}$ by its MLE calculated as (12), inserting (38) into (36), and neglecting the constant items leads to the persymmetric Wald detector in the subspace interference condition given by

$$t_{\text{PS - Wald - I}} = \frac{\operatorname{tr}(\widetilde{\boldsymbol{Y}}^{\mathrm{H}} \boldsymbol{P}^{\mathrm{H}}_{\widetilde{\boldsymbol{H}}_p|\widetilde{\boldsymbol{G}}_p} \boldsymbol{P}_{\widetilde{\boldsymbol{H}}_p|\widetilde{\boldsymbol{G}}_p} \widetilde{\boldsymbol{Y}})}{\operatorname{tr}(\widetilde{\boldsymbol{Y}}^{\mathrm{H}} \boldsymbol{P}^{\perp}_{\widetilde{\boldsymbol{S}}_p} \widetilde{\boldsymbol{Y}})} = \frac{\left\| \boldsymbol{P}_{\widetilde{\boldsymbol{H}}_p|\widetilde{\boldsymbol{G}}_p} \widetilde{\boldsymbol{Y}} \right\|_{\mathrm{F}}^2}{\left\| \boldsymbol{P}^{\perp}_{\widetilde{\boldsymbol{S}}_p} \widetilde{\boldsymbol{Y}} \right\|_{\mathrm{F}}^2} \tag{40}$$

where $\widetilde{\boldsymbol{S}}_p = \widehat{\boldsymbol{R}}_p^{-1/2} \boldsymbol{S}_p$.

3.3 Discussions

In the following, we investigate the signal operation and CFAR property of the proposed detectors.

The signal flow of the proposed PS-Rao-I and PS-Wald-I detectors is shown in Fig. 1, where the red lines indicate the signal flow for matrix projection.

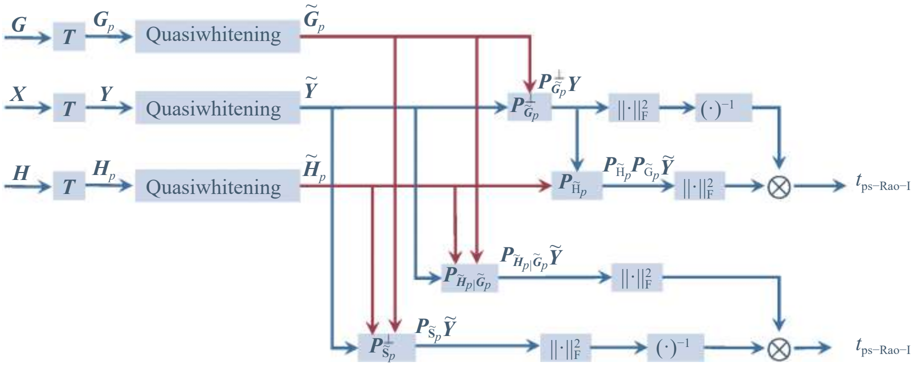

Fig. 1 Block diagram of PS-Rao-I and PS-Wald-I detector.

(i) Numerator of Test Statistic: The numerator of both tests represents the energy of the transformed signal after subspace projection which, unlike their interference-free counterparts, differs from each other. Specifically, the PS-Rao-I projects the transformed signal $\widetilde{\boldsymbol{Y}}$ successively into the orthogonal complement of the quasi-whitened interference subspace (via $\boldsymbol{P}^{\perp}_{\widetilde{\boldsymbol{G}}_p}$) which rejects the interference, and the quasi-whitened signal subspace (via $\boldsymbol{P}_{\widetilde{\boldsymbol{H}}_p}$) which combines the signal. The PS-Wald-I, on the other hand, projects $\widetilde{\boldsymbol{Y}}$ into the transformed signal subspace along the transformed interference subspace via oblique projection matrix $\boldsymbol{P}_{\widetilde{\boldsymbol{H}}_p|\widetilde{\boldsymbol{G}}_p}$, which achieves interference elimination and signal combination simultaneously.

(ii) Denominator of Test Statistic: The denominator of the two detectors also differs from each other. The PS-Rao-I test computes the denominator from the transformed signal after projection into the orthogonal complement of the quasi-whitened interference subspace, which does not contain the interference and therefore corresponds to the calculation of γ under H_0 situation, while the PS-Wald-I test computes the denominator from the transformed signal after projection into the orthogonal complement of the quasi-whitened noise plus interference subspace, which cancels both the signal and the interference, and in consequence corresponds to the calculation of γ under H_1 situation.

It is worth highlighting that both detectors (the PS-Rao-I and the PS-Wald-I) are CFAR w.r.t. the covariance matrix $\boldsymbol{R}$ and γ. The CFARness of the PS-Rao-I test can be proved in a manner similar to [19]. For brevity, we will not explore it in this article.

The CFAR property of the PS-Wald-I detector is investigated and discussed in the following. Since the CFAR property will not be affected by the trace operator, we first rewrite (40) as

$$t_{\text{PS - Wald - I}} = \frac{\operatorname{tr}(\boldsymbol{\varPsi}_1)}{\operatorname{tr}(\boldsymbol{\varPsi}_2)} \tag{41}$$

where

$$\boldsymbol{\varPsi}_1 = \gamma \bar{\boldsymbol{Y}}_0^{\mathrm{H}} \bar{\boldsymbol{F}} \bar{\boldsymbol{H}}_p (\bar{\boldsymbol{H}}_p^{\mathrm{H}} \bar{\boldsymbol{F}} \bar{\boldsymbol{H}}_p)^{-1} \bar{\boldsymbol{H}}_p^{\mathrm{H}} \bar{\boldsymbol{R}}^{-1} \bar{\boldsymbol{H}}_p \cdot (\bar{\boldsymbol{H}}_p^{\mathrm{H}} \bar{\boldsymbol{F}} \bar{\boldsymbol{H}}_p)^{-1} \bar{\boldsymbol{H}}_p^{\mathrm{H}} \bar{\boldsymbol{F}} \bar{\boldsymbol{Y}}_0, \tag{42}$$

$$\boldsymbol{\varPsi}_2 = \gamma \left[\bar{\boldsymbol{Y}}_0^{\mathrm{H}} \bar{\boldsymbol{R}}^{-1} \bar{\boldsymbol{Y}}_0 - \bar{\boldsymbol{Y}}_0^{\mathrm{H}} \bar{\boldsymbol{R}}^{-1} \bar{\boldsymbol{S}}_p (\bar{\boldsymbol{S}}_p^{\mathrm{H}} \bar{\boldsymbol{R}}^{-1} \bar{\boldsymbol{S}}_p)^{-1} \bar{\boldsymbol{S}}_p^{\mathrm{H}} \bar{\boldsymbol{R}}^{-1} \bar{\boldsymbol{Y}}_0 \right], \tag{43}$$

$$\begin{cases} \bar{\boldsymbol{F}} = \boldsymbol{R}^{1/2} \boldsymbol{F} \boldsymbol{R}^{1/2} \\ \bar{\boldsymbol{G}}_p = \boldsymbol{R}^{-1/2} \boldsymbol{G}_p \end{cases} \tag{44}$$

with

$$\boldsymbol{F} = \widehat{\boldsymbol{R}}_p^{-1} - \widehat{\boldsymbol{R}}_p^{-1} \boldsymbol{G}_p (\boldsymbol{G}_p^{\mathrm{H}} \widehat{\boldsymbol{R}}_p^{-1} \boldsymbol{G}_p)^{-1} \boldsymbol{G}_p^{\mathrm{H}} \widehat{\boldsymbol{R}}_p^{-1}. \tag{45}$$

It is observed that the ratio of $\boldsymbol{\varPsi}_1$ to $\boldsymbol{\varPsi}_2$ cancels their dependence on γ, which suggests the CFARness of the PS-Wald-I detector with respect to γ under hypothesis H_0.

In the following, we show the CFARness of (41) with respect to $\boldsymbol{R}$ under H_0. Let $\dot{\boldsymbol{U}} \triangleq [\bar{\boldsymbol{G}}_{p//}, \bar{\boldsymbol{G}}_{p_\perp}]$ be a unitary matrix, with $\bar{\boldsymbol{G}}_{p//} = \bar{\boldsymbol{G}}_p (\bar{\boldsymbol{G}}_p^{\mathrm{H}} \bar{\boldsymbol{G}}_p)^{-1}$ and $\bar{\boldsymbol{G}}_{p_\perp}^{\mathrm{H}} \bar{\boldsymbol{G}}_{p//} = \boldsymbol{0}_{(N-s)\times s}$. Define

$$\begin{cases} \bar{\boldsymbol{Y}}_{\dot{U}} \triangleq \dot{\boldsymbol{U}}^{\rm H}\bar{\boldsymbol{Y}}_0 \\ \bar{\boldsymbol{F}}_{\dot{U}} \triangleq \dot{\boldsymbol{U}}^{\rm H}\bar{\boldsymbol{F}}\dot{\boldsymbol{U}} \\ \bar{\boldsymbol{H}}_{\dot{U}\dot{U}} \triangleq \dot{\boldsymbol{U}}^{\rm H}\bar{\boldsymbol{H}}_p \\ \bar{\boldsymbol{R}}_{\dot{U}} \triangleq \dot{\boldsymbol{U}}^{\rm H}\bar{\boldsymbol{R}}\dot{\boldsymbol{U}} \end{cases}. \tag{46}$$

After some matrix manipulation, we can express $\boldsymbol{\varPsi}_1$ as

$$\begin{aligned}\boldsymbol{\varPsi}_1 = \gamma\bar{\boldsymbol{Y}}_{\dot{U}}^{\rm H}\bar{\boldsymbol{F}}_{\dot{U}}\bar{\boldsymbol{H}}_{\dot{U}}(\bar{\boldsymbol{H}}_{\dot{U}}^{\rm H}\bar{\boldsymbol{F}}_{\dot{U}}\bar{\boldsymbol{H}}_{\dot{U}\dot{U}})^{-1}\bar{\boldsymbol{H}}_{\dot{U}}^{\rm H}\bar{\boldsymbol{R}}_{\dot{U}}^{-1}\cdot \\ \bar{\boldsymbol{H}}_{\dot{U}\dot{U}}(\bar{\boldsymbol{H}}_{\dot{U}}^{\rm H}\bar{\boldsymbol{F}}_{\dot{U}}\bar{\boldsymbol{H}}_{\dot{U}\dot{U}})^{-1}\bar{\boldsymbol{H}}_{\dot{U}}^{\rm H}\bar{\boldsymbol{F}}_{\dot{U}}\bar{\boldsymbol{Y}}_{\dot{U}} = \\ \gamma\bar{\boldsymbol{Y}}_2^{\rm H}\bar{\boldsymbol{R}}_{22}^{-1}\bar{\boldsymbol{H}}_2(\bar{\boldsymbol{H}}_2^{\rm H}\bar{\boldsymbol{R}}_{22}^{-1}\bar{\boldsymbol{H}}_2)^{-1}\bar{\boldsymbol{H}}_{\dot{U}}^{\rm H}\bar{\boldsymbol{R}}_{\dot{U}}^{-1}\bar{\boldsymbol{H}}_{\dot{U}\dot{U}}\cdot \\ (\bar{\boldsymbol{H}}_2^{\rm H}\bar{\boldsymbol{R}}_{22}^{-1}\bar{\boldsymbol{H}}_2)^{-1}\bar{\boldsymbol{H}}_2^{\rm H}\bar{\boldsymbol{R}}_{22}^{-1}\bar{\boldsymbol{Y}}_2\end{aligned} \tag{47}$$

where $\bar{\boldsymbol{Y}}_{\dot{U}} \triangleq \begin{bmatrix}\bar{\boldsymbol{Y}}_1^{\rm T} & \bar{\boldsymbol{Y}}_2^{\rm T}\end{bmatrix}^{\rm T}$, $\bar{\boldsymbol{H}}_{\dot{U}} \triangleq \begin{bmatrix}\bar{\boldsymbol{H}}_1^{\rm T} & \bar{\boldsymbol{H}}_2^{\rm T}\end{bmatrix}^{\rm T}$ and $\bar{\boldsymbol{R}}_{\dot{U}} \triangleq \begin{bmatrix}\bar{\boldsymbol{R}}_{11}, \bar{\boldsymbol{R}}_{12}; \bar{\boldsymbol{R}}_{21}, \bar{\boldsymbol{R}}_{22}\end{bmatrix}$. The dimensions of $\bar{\boldsymbol{Y}}_2$, $\bar{\boldsymbol{R}}_{22}$ and $\bar{\boldsymbol{H}}_2$ are $(N-s)\times L$, $(N-s)\times(N-s)$ and $(N-s)\times r$, respectively. It can be verified that under $\rm H_0$

$$\bar{\boldsymbol{Y}}_2 \sim {\rm CN}(\boldsymbol{0}_{(N-s)\times L}, \boldsymbol{I}_{N-s}), \tag{48}$$

and

$$\bar{\boldsymbol{R}}_{22} \sim {\rm CW}(K, \boldsymbol{I}_{N-s}). \tag{49}$$

Let $\boldsymbol{V} = [\bar{\boldsymbol{H}}_{2//}, \bar{\boldsymbol{H}}_{2\perp}]$ be a unitary matrix, with $\bar{\boldsymbol{H}}_{2//} = \bar{\boldsymbol{H}}_2(\bar{\boldsymbol{H}}_2^{\rm H}\bar{\boldsymbol{H}}_2)^{-1}$ and $\bar{\boldsymbol{H}}_{2_\perp}^{\rm H}\bar{\boldsymbol{H}}_{2//} = \boldsymbol{0}_{(N-s-r)\times r}$. Define

$$\begin{cases} \bar{\boldsymbol{Y}}_{2V} \triangleq \boldsymbol{V}^{\rm H}\bar{\boldsymbol{Y}}_2 \\ \bar{\boldsymbol{R}}_{22V} \triangleq \boldsymbol{V}^{\rm H}\bar{\boldsymbol{R}}_{22}\boldsymbol{V} \\ \boldsymbol{E}_1 = \boldsymbol{V}^{\rm H}\bar{\boldsymbol{H}}_2 \end{cases}. \tag{50}$$

$\boldsymbol{\varPsi}_1$ can be reformulated as

$$\begin{aligned}\boldsymbol{\varPsi}_1 = \gamma\bar{\boldsymbol{Y}}_{2V}^{\rm H}\bar{\boldsymbol{R}}_{22V}^{-1}\boldsymbol{E}_1(\boldsymbol{E}_1^{\rm H}\bar{\boldsymbol{R}}_{22V}^{-1}\boldsymbol{E}_1)^{-1}\bar{\boldsymbol{H}}_{\dot{U}}^{\rm H}\bar{\boldsymbol{R}}_{\dot{U}}^{-1}\bar{\boldsymbol{H}}_{\dot{U}}\cdot \\ (\boldsymbol{E}_1^{\rm H}\bar{\boldsymbol{R}}_{22V}^{-1}\boldsymbol{E}_1)^{-1}\boldsymbol{E}_1^{\rm H}\bar{\boldsymbol{R}}_{22V}^{-1}\bar{\boldsymbol{Y}}_{2V}.\end{aligned} \tag{51}$$

It can be verified that under $\rm H_0$

$$\bar{\boldsymbol{Y}}_{2V} \sim {\rm CN}(\boldsymbol{0}_{(N-s)\times L}, \boldsymbol{I}_{N-s}), \tag{52}$$

$$\bar{\boldsymbol{R}}_{22V} \sim {\rm CW}(K, \boldsymbol{I}_{N-s}), \tag{53}$$

and

$$\boldsymbol{E}_1 = \begin{bmatrix} \boldsymbol{I}_r \\ \boldsymbol{0}_{(N-r-s)\times r} \end{bmatrix} \tag{54}$$

which suggests that both $\bar{\boldsymbol{Y}}_{2V}^{\rm H}\bar{\boldsymbol{R}}_{22V}^{-1}\boldsymbol{E}_1$ and $\boldsymbol{E}_1^{\rm H}\bar{\boldsymbol{R}}_{22V}^{-1}\boldsymbol{E}_1$ are independent of $\boldsymbol{R}$ under hypothesis $\rm H_0$.

Let $\dot{\boldsymbol{V}} \triangleq [\bar{\boldsymbol{H}}_{\dot{U}//}, \bar{\boldsymbol{H}}_{\dot{U}\perp}]$ be a unitary matrix, with $\bar{\boldsymbol{H}}_{\dot{U}//} = \bar{\boldsymbol{H}}_{\dot{U}}(\bar{\boldsymbol{H}}_{\dot{U}}^{\rm H}\bar{\boldsymbol{H}}_{\dot{U}})^{-1}$ and $\bar{\boldsymbol{H}}_{\dot{U}\perp}\bar{\boldsymbol{H}}_{\dot{U}//} = \boldsymbol{0}_{(N-r)\times r}$. By implementing unitary transformation on $\bar{\boldsymbol{H}}_{\dot{U}}$ and $\bar{\boldsymbol{R}}_{\dot{U}}^{-1}$, $\boldsymbol{\varPsi}_1$ can be reformulated as

$$\begin{aligned}\boldsymbol{\varPsi}_1 = \gamma\bar{\boldsymbol{Y}}_{2V}^{\rm H}\bar{\boldsymbol{R}}_{22V}^{-1}\boldsymbol{E}_1(\boldsymbol{E}_1^{\rm H}\bar{\boldsymbol{R}}_{22V}^{-1}\boldsymbol{E}_1)^{-1}\boldsymbol{E}_2^{\rm H}\bar{\boldsymbol{R}}_{\dot{U}\dot{V}}^{-1}\boldsymbol{E}_2\cdot \\ (\boldsymbol{E}_1^{\rm H}\bar{\boldsymbol{R}}_{22V}^{-1}\boldsymbol{E}_1)^{-1}\boldsymbol{E}_1^{\rm H}\bar{\boldsymbol{R}}_{22V}^{-1}\bar{\boldsymbol{Y}}_{2V}\end{aligned} \tag{55}$$

where $\bar{\boldsymbol{R}}_{\dot{U}\dot{V}} = \dot{\boldsymbol{V}}^{\rm H}\bar{\boldsymbol{R}}_{\dot{U}}\dot{\boldsymbol{V}}$ and

$$\boldsymbol{E}_2 = \begin{bmatrix} \boldsymbol{I}_r \\ \boldsymbol{0}_{(N-r)\times r} \end{bmatrix}. \tag{56}$$

It follows that $\boldsymbol{E}_2^{\rm H}\bar{\boldsymbol{R}}_{\dot{U}\dot{V}}^{-1}\boldsymbol{E}_2$ is independent of $\boldsymbol{R}$. Gathering the above information, we can conclude that $\boldsymbol{\varPsi}_1$ is independent of $\boldsymbol{R}$.

We then proceed to show the statistical independence of $\boldsymbol{\varPsi}_2$ on $\boldsymbol{R}$. Let $\boldsymbol{U}' \triangleq \begin{bmatrix}\bar{\boldsymbol{S}}_{p//}, \bar{\boldsymbol{S}}_{p\perp}\end{bmatrix}$ be a unitary matrix, with $\bar{\boldsymbol{S}}_{p//} = \bar{\boldsymbol{S}}_p(\bar{\boldsymbol{S}}_p^{\rm H}\bar{\boldsymbol{S}}_p)^{-1}$, $\bar{\boldsymbol{S}}_{p\perp}^{\rm H}\bar{\boldsymbol{S}}_{p//} = \boldsymbol{0}_{(N-r-s)\times(r+s)}$. By implementing unitary transformation on $\bar{\boldsymbol{H}}_{\dot{U}}$ and $\bar{\boldsymbol{R}}_{\dot{U}}^{-1}$, $\boldsymbol{\varPsi}_2$ can be reformulated as

$$\begin{aligned}\boldsymbol{\varPsi}_2 = \gamma[\bar{\boldsymbol{Y}}_0^{\rm H}\bar{\boldsymbol{R}}^{-1}\bar{\boldsymbol{Y}}_0 - \\ \bar{\boldsymbol{Y}}_{U'}^{\rm H}\bar{\boldsymbol{R}}_{U'}^{-1}\boldsymbol{E}_S(\boldsymbol{E}_S^{\rm H}\bar{\boldsymbol{R}}_{U'}^{-1}\boldsymbol{E}_S)^{-1}\boldsymbol{E}_S^{\rm H}\bar{\boldsymbol{R}}_{U'}^{-1}\bar{\boldsymbol{Y}}_{U'}]\end{aligned} \tag{57}$$

where $\bar{\boldsymbol{Y}}_{U'} \triangleq \boldsymbol{U}'^{\rm H}\bar{\boldsymbol{Y}}_0$, $\bar{\boldsymbol{R}}_{U'} = \boldsymbol{U}'^{\rm H}\boldsymbol{R}\bar{\boldsymbol{U}}'$, and

$$\boldsymbol{E}_S \triangleq \boldsymbol{U}'^{\rm H}\bar{\boldsymbol{S}}_p = \begin{bmatrix} \boldsymbol{I}_{r+s} \\ \boldsymbol{0}_{(N-r-s)\times(r+s)} \end{bmatrix}. \tag{58}$$

It can be verified that under hypothesis $\rm H_0$

$$\bar{\boldsymbol{Y}}_{U'} \sim {\rm CN}(\boldsymbol{0}_{N\times L}, \boldsymbol{I}_N), \tag{59}$$

$$\bar{\boldsymbol{R}}_{U'} \sim {\rm CW}(K, \boldsymbol{I}_N). \tag{60}$$

On the basis of the above derivation, we can conclude that $\boldsymbol{\varPsi}_2$ is independent of $\boldsymbol{R}$ under hypothesis $\rm H_0$. Therefore, the CFARness of the PS-Wald-I follows.

4. Numerical results

We now consider the target detection problem in the presence of subspace interference in the PHE, and develop the corresponding PS-Rao-I and PS-Wald-I detector.

4.1 Simulation results

We now present numerical examples to verify our analysis and compare the proposed persymmetric detectors. In the following simulations, we set $N = 8$, $L = 4$. Let $\boldsymbol{\Delta}$ be an exponentially correlated covariance matrix with one-lag correlation coefficient $\rho = 0.9$, i.e., the (i, j)th element of the noise covariance matrix $\boldsymbol{\Delta}$ is set to $\rho^{|i-j|}$. In this paper, we define the signal to noise ratio (SNR) and the interference to noise ratio (INR) as

$${\rm SNR} = {\rm tr}(\boldsymbol{B}^{\rm H}\boldsymbol{H}^{\rm H}\boldsymbol{\Delta}^{-1}\boldsymbol{H}\boldsymbol{B}), \tag{61}$$

$${\rm INR} = {\rm tr}(\boldsymbol{Q}^{\rm H}\boldsymbol{G}^{\rm H}\boldsymbol{\Delta}^{-1}\boldsymbol{G}\boldsymbol{Q}). \tag{62}$$

Column vectors of $\boldsymbol{H}$ and $\boldsymbol{G}$ are respectively given by

$$\boldsymbol{h}_i = \frac{1}{\sqrt{N}}[1, {\rm e}^{-{\rm j}2\pi f_i}, \cdots, {\rm e}^{-{\rm j}2\pi f_i(N-1)}]^{\rm T}, i = 1, 2, \cdots, r, \tag{63}$$

$$\boldsymbol{g}_i = \frac{1}{\sqrt{N}}[1, \mathrm{e}^{-\mathrm{j}2\pi g_i}, \cdots, \mathrm{e}^{-\mathrm{j}2\pi g_i(N-1)}]^{\mathrm{T}}, i = 1, 2, \cdots, s. \tag{64}$$

In the following, we conduct simulations for the subspace interference condition under matched assumptions. A total of 100/Pfa Monte Carlo (MC) trials are used to obtain the simulated performance, where Pfa is the false alarm probability. If not otherwise specified, Pfa $= 10^{-3}$, $\gamma = 0.5$, $r = 3$, $s = 2$, $f_1 = 0.09$, $f_2 = 0.1$, $f_3 = 0.11$, $g_1 = -0.09$, and $g_2 = -0.08$ throughout the paper. For the sake of comparison, we also provide the performance of the Rao, Wald, 2S-Rao and 2S-Wald tests. Precisely, for the problem in (1), the Rao test and the 2S-Rao test are respectively given by [16]

$$t_{\text{Rao-I}} = \mathrm{tr}(\bar{\bar{\boldsymbol{X}}}^{\mathrm{H}} \mathbf{P}^{\perp}_{\bar{\bar{G}}} \mathbf{P}_{\bar{\bar{H}}} \mathbf{P}^{\perp}_{\bar{\bar{G}}} \bar{\bar{\boldsymbol{X}}}) / \widehat{\gamma}_0, \tag{65}$$

$$t_{\text{2S - Rao - I}} = \mathrm{tr}(\widetilde{\boldsymbol{X}}^{\mathrm{H}} \boldsymbol{P}^{\perp}_{\widetilde{\boldsymbol{G}}} \boldsymbol{P}_{\widetilde{\boldsymbol{H}}} \boldsymbol{P}^{\perp}_{\widetilde{\boldsymbol{G}}} \widetilde{\boldsymbol{X}}) / \mathrm{tr}(\widetilde{\boldsymbol{X}}^{\mathrm{H}} \boldsymbol{P}^{\perp}_{\widetilde{\boldsymbol{G}}} \widetilde{\boldsymbol{X}}). \tag{66}$$

Adopting similar derivation procedure proposed in Subsection 3.2 for the problem in (1), results in the Wald test and the 2S-Wald test given below

$$t_{\text{Wald - I}} = \mathrm{tr}\left(\breve{\boldsymbol{X}}^{\mathrm{H}} \boldsymbol{P}^{\mathrm{H}}_{\breve{\boldsymbol{H}}|\breve{\boldsymbol{G}}} \boldsymbol{P}_{\breve{\boldsymbol{H}}|\breve{\boldsymbol{G}}} \breve{\boldsymbol{X}}\right) / \hat{\gamma}_1 \tag{67}$$

$$t_{\text{2S - Wald - I}} = \mathrm{tr}\left(\tilde{\boldsymbol{X}}^{\mathrm{H}} \boldsymbol{P}^{\mathrm{H}}_{\tilde{\boldsymbol{H}}|\tilde{\boldsymbol{G}}} \boldsymbol{P}_{\tilde{\boldsymbol{H}}|\tilde{\boldsymbol{G}}} \tilde{\boldsymbol{X}}\right) \Big/ \mathrm{tr}\left(\tilde{\boldsymbol{X}}^{\mathrm{H}} \boldsymbol{P}^{\perp}_{\tilde{\boldsymbol{S}}}\right) \tag{68}$$

where

$$\begin{cases} \bar{\bar{\mathbf{X}}} = \widehat{\mathbf{R}}_0^{-1/2}\mathbf{X} \\ \breve{\boldsymbol{X}} = \widehat{\mathbf{R}}_1^{-1/2}\mathbf{X} \\ \tilde{\mathbf{X}} = \mathbf{M}^{-1/2}\mathbf{X} \end{cases}, \tag{69}$$

$$\begin{cases} \bar{\bar{\mathbf{H}}} = \widehat{\mathbf{R}}_0^{-1/2}\mathbf{H} \\ \breve{\boldsymbol{H}} = \widehat{\mathbf{R}}_1^{-1/2}\mathbf{H} \\ \mathbf{H} = \mathbf{H}^{-1/2}\mathbf{H} \end{cases}, \tag{70}$$

$$\begin{cases} \bar{\bar{\mathbf{G}}} = \widehat{\mathbf{R}}_0^{-1/2}\mathbf{G} \\ \breve{\boldsymbol{G}} = \widehat{\mathbf{R}}_1^{-1/2}\mathbf{G} \\ \mathbf{G} = \mathbf{M}^{-1/2}\mathbf{G} \end{cases} \tag{71}$$

are the square-root matrix of $\widehat{\boldsymbol{R}}_0$ and $\widehat{\boldsymbol{R}}_1$, respectively,

$$\widehat{\boldsymbol{R}}_0 = \boldsymbol{M}^{1/2}(\boldsymbol{I}_N + \boldsymbol{P}^{\perp}_{\widetilde{\boldsymbol{G}}} \widetilde{\boldsymbol{X}} \widetilde{\boldsymbol{X}}^{\mathrm{H}} \boldsymbol{P}^{\perp}_{\widetilde{\boldsymbol{G}}} / \hat{\gamma}_0) \boldsymbol{M}^{1/2} \Big/ (K+L), \tag{72}$$

$$\widehat{\boldsymbol{R}}_1 = \boldsymbol{M}^{1/2}(\boldsymbol{I}_N + \boldsymbol{P}^{\perp}_{\widetilde{\boldsymbol{S}}} \widetilde{\boldsymbol{X}} \widetilde{\boldsymbol{X}}^{\mathrm{H}} \boldsymbol{P}^{\perp}_{\widetilde{\boldsymbol{S}}} / \hat{\gamma}_1) \boldsymbol{M}^{1/2} \Big/ (K+L). \tag{73}$$

$\hat{\gamma}_0$ and $\hat{\gamma}_1$ are the unique positive solutions of the following equation:

$$\frac{NL}{K+L} - \sum_{k=1}^{r} \frac{\lambda_{k,i}}{\lambda_{k,i} + x} = 0 \tag{74}$$

where $r = \min(N, L)$, x denotes the unknown, $\lambda_{k,0}$ and $\lambda_{k,1}$ are the kth nonzero eigenvalue of $\widetilde{\boldsymbol{X}}^{\mathrm{H}} \boldsymbol{P}^{\perp}_{\widetilde{\boldsymbol{G}}} \widetilde{\boldsymbol{X}}$ and $\widetilde{\boldsymbol{X}}^{\mathrm{H}} \boldsymbol{P}^{\perp}_{\widetilde{\boldsymbol{S}}} \widetilde{\boldsymbol{X}}$, respectively.

The detection probability (Pd) versus SNR is shown in Fig. 2. The INR is set to be 20 dB. As can be seen from Fig. 2, the proposed PS-Rao-I and PS-Wald-I outperform their conventional counterparts under the condition of limited training support. Specifically, for $K = 9$, the conventional Rao-I, Wald-I, 2S-Rao-I and 2S-Wald-I detectors, show performance degradation, while the proposed PS-Rao-I and PS-Wald-I keep being at a higher detection probability. In particular, PS-Rao-I show a better detection performance than PS-Wald-I at low SNR, which corresponds well to the fact that the Rao test is originally proposed as a weak signal approximation for the GLRT [49]. With the increase of K, the performance gap between the proposed detectors and the traditional ones becomes smaller. It is also observed from Fig. 2 that the Pd of the Rao test is not a monotonically increasing function of the SNR, which is consistent with that in [19]. The receiver operating characteristic (ROC) curves of the above mentioned detectors are presented in Fig. 3, where we set $K = 9$, SNR $= 20$ dB, and INR $= 20$ dB. It can be seen that the results observed from Fig. 3 are consistent with those in Fig. 2.

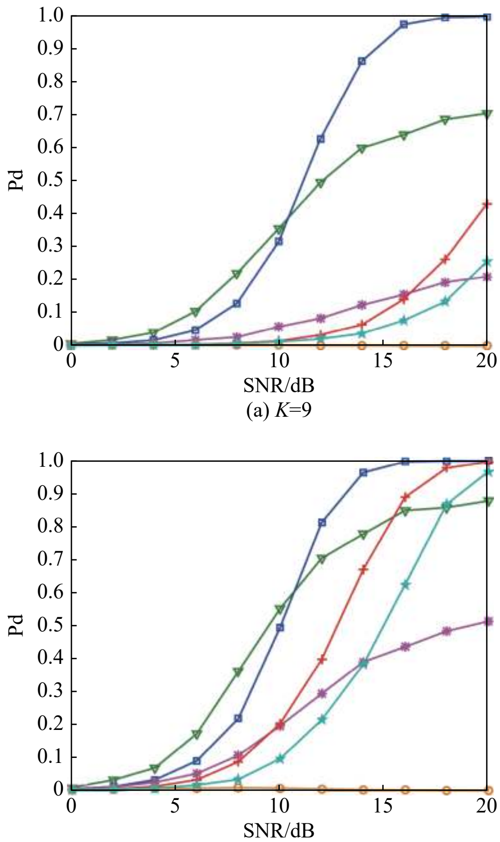

(a) K=9

(b) K=12

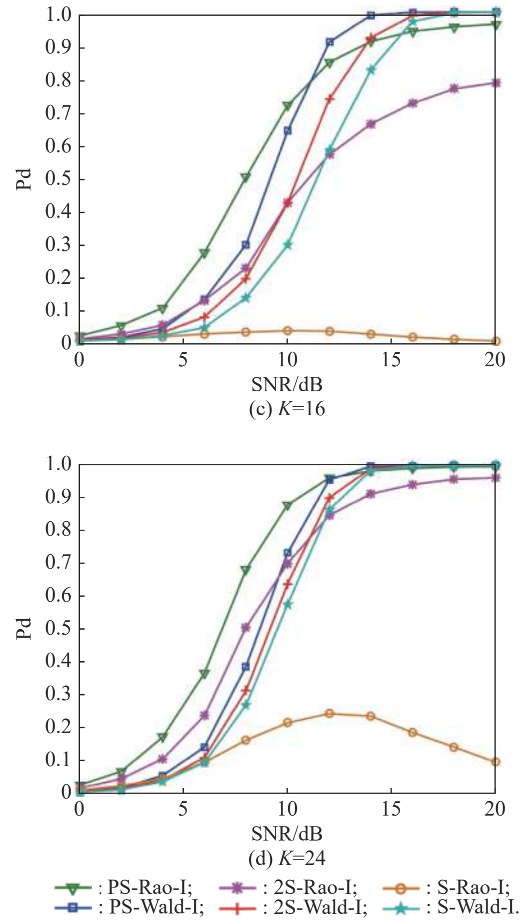

Fig. 2 Probability of detection versus SNR when *N*=8, *L*=4, *γ*=0.5, *r*=3, *s*=2, Pfa=10^{-3} and INR=20 dB

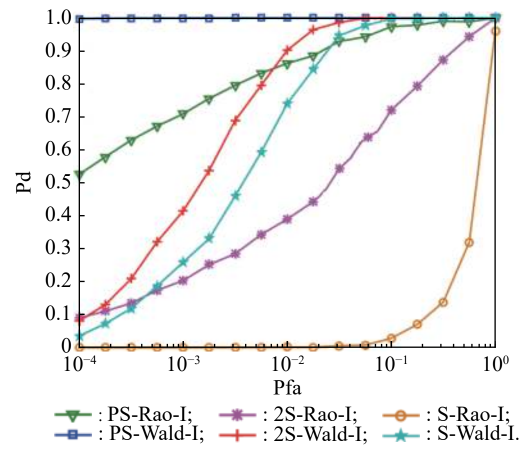

Fig. 3 ROC curves for *N*=8, *L*=4, *K*=9, *γ*=0.5, *r*=3, *s*=2, SNR=20 dB and INR=20 dB

Fig. 4 displays the performance of the detectors under different INRs. It is seen that the probability of detection of the detectors in Fig. 4 are not affected by the change of the INR, suggesting that these detectors can effectively reject the directional interference.

Fig. 5 depicts the detection thresholds and Pd of PS-Rao-I and PS-Wald-I under different γ. The results in Fig. 5 (a) show that the detection thresholds do not vary with the change of the power scaling factor, which is consistent with CFAR analysis presented in Subsection 3.3. It is seen from Fig. 5(b) that all detectors exhibit decreased probability of detection while increasing γ. In this case, the PS-Rao-I and PS-Wald-I can still exhibit a better performance than the other conventional counterparts.

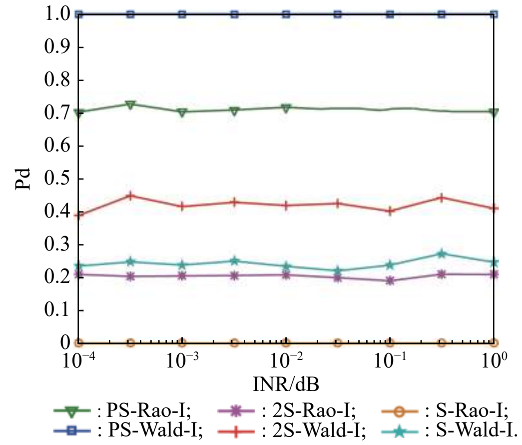

Fig. 4 Probability of detection versus INR when *N*=8, *L*=4, *K*=9, *γ*=0.5, *r*=3, *s*=2, Pfa=10^{-3} and SNR=20 dB

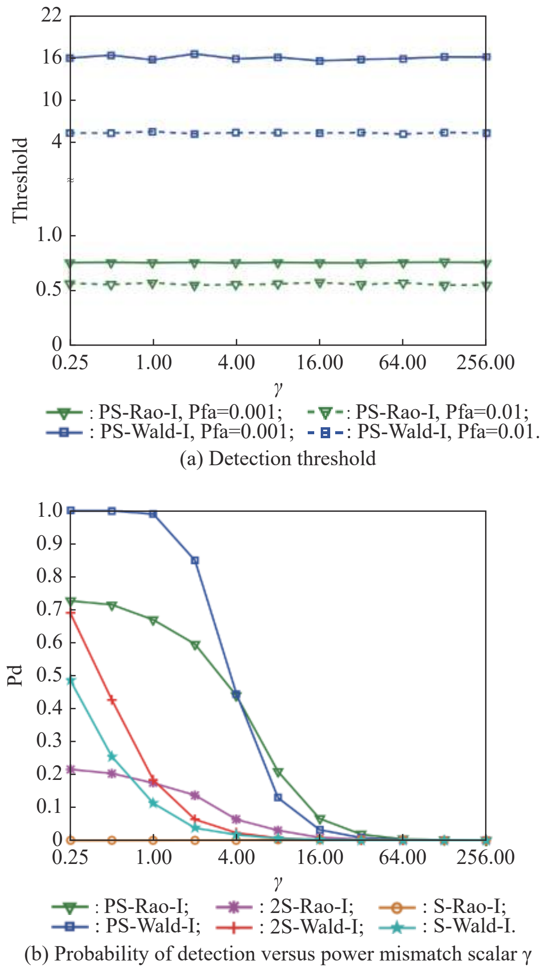

Fig. 5 Detection thresholds and Pd of PS-Rao-I and PS-Wald-I under different *γ*, *N*=8, *K*=9, SNR=20 dB and INR=20 dB

On the other hand, we also compare the proposed detector with GLRT-based detectors that utilize persymmetry [38] (referred to as PS-GLRT-IP) and [46] (referred to as PS-GLRT-I). The simulation result is shown in Fig. 6. For smaller sample support, PS-GLRT-I shows the best detection performance and the proposed PS-Rao-I show better detection performance than PS-Wald-I and PS-GLRT-IP at low SNR. As K increases, the proposed PS-Rao-I shows a better detection performance at most SNR region, especially for low SNR. In addition, the performance gap between the PS-Wald-I and PS-GLRT-IP and the PS-GLRT-I becomes rather small. Comparing with the GLRT-based persymmetric detectors, the PS-Wald-I does not have a greater advantage in detection probability for small sample support and high SNR. However, it has the advantage of reducing the computational burden as it only needs to estimate the unknown parameters under H_1 hypothesis.

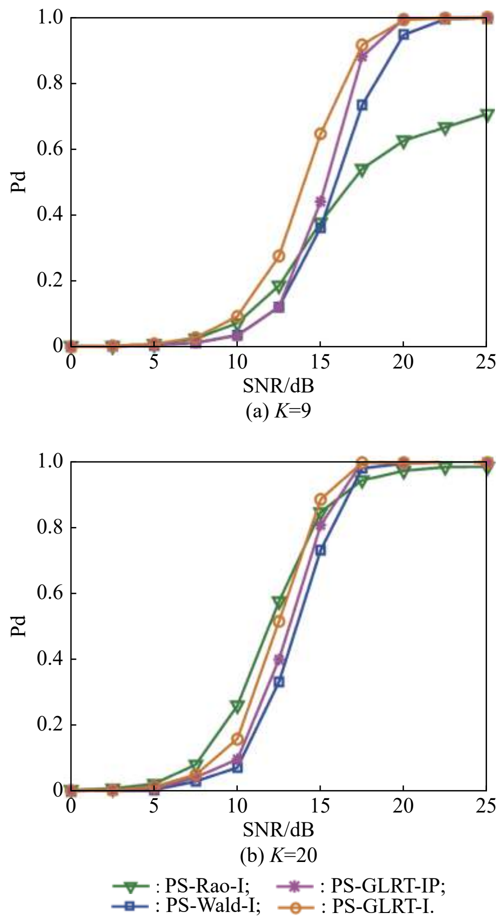

Fig. 6 Probability of detection versus SNR when N=8, L=4, γ=1.5, r=3, s=2, Pfa=10^{-3} and INR=20 dB

4.2 Experimental Results

In the following we evaluate the performance of the proposed detectors using measured data collected by an airborne radar in China. The real data contains 89 538 pulses and 280 range cells. Due to the limited amount of real data, we set $N=8$ and Pfa $=10^{-2}$. Range cells 10−11 of the real data are chosen as the primary data, and range cells adjacent to the primary data are regarded as the training data, i.e., range cells 4−7 and 12−16 for $K=9$, and range cells 4−7 and 12−17 for $K=10$. Fig. 7 shows fitting results of the clutter amplitude for the primary data with the Rayleigh distribution. It is obviously seen that the real data is not Gaussian clutter.

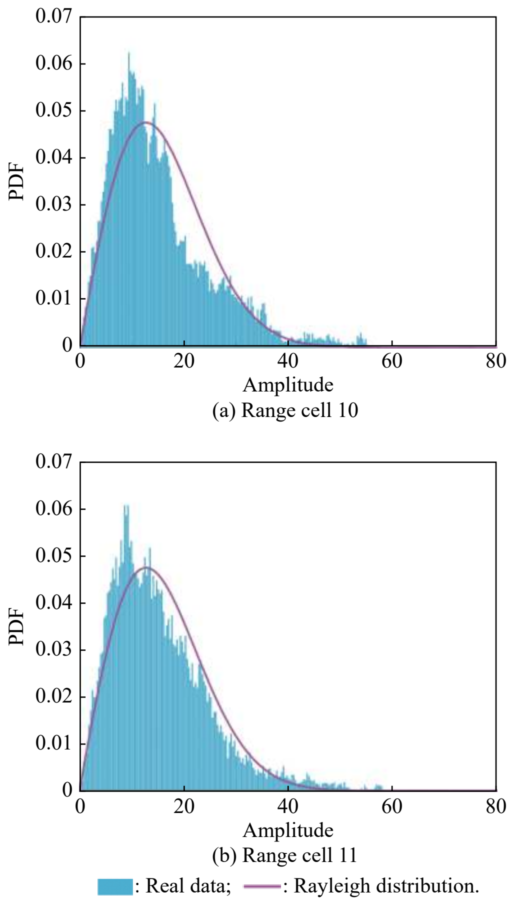

Fig. 7 Fitting results of the clutter amplitude of the primary data with the Rayleigh distribution

Then, the detection performance of the proposed detector is assessed. Without loss of generality, we insert a range-spread target signal with $r=3$ into range cells 10−11. An interference with $s=1$, and INR = 20 dB are supposed in the primary data. The SNR and INR are respectively defined as

$$\text{SNR} = \sum\nolimits_{l=1}^{L} \sigma_{s,l}^2 / \sigma_c^2, \tag{75}$$

$$\text{INR} = \sum\nolimits_{l=1}^{L} \sigma_{j,l}^2 / \sigma_c^2, \tag{76}$$

with σ_c^2 being the average clutter power.

The number of MC trials for calculating the probability of false alarm is 10 000 and the number of MC trials for calculating the probability of detection is 5 000. Fig. 8 shows the probability of detection versus SNR for the experimental dataset for cases of $K=9$ and $K=10$. It is seen that PS-Wald-I achieves a significantly better performance than 2S-Rao-I, 2S-Wald-I, Rao-I and Wald-I, and is slightly worse than PS-Rao-I at low SNR, which coincides with the results in Fig. 2.

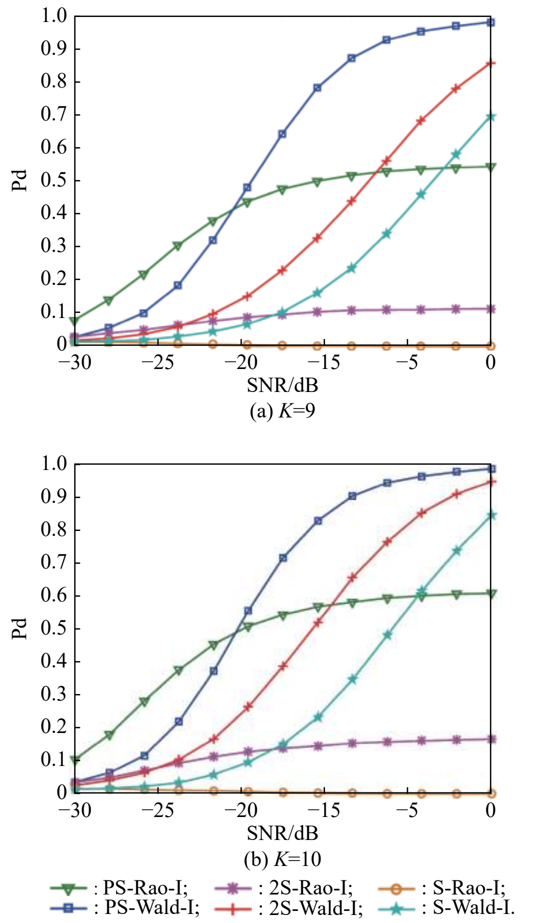

Fig. 8 Probability of detection versus SNR for experimental dataset when N=8, L=2, r=3, s=1, Pfa=10^{-2} and INR=20 dB

5. Conclusions

In this paper, we investigate range-spread target detection in subspace interference and non-homogeneous noise with small training support. With the help of unitary transformation, two detectors are designed, namely the PS-Rao-I and PS-Wald-I, which incorporate the persymmetric structure of the disturbance covariance matrix into the detector design. The block diagrams for the proposed detectors are presented to demonstrate the signal flow of each detector. In particular, the PS-Rao-I rejects interference and integrate signal successively through separated matrix projection, while the PS-Wald-I achieves interference elimination and signal combination simultaneously via oblique projection. Both detectors are shown to be CFAR with respect to the unknown covariance matrix and the power scaling factor. Numerical examples and experimental results indicate that the proposed detectors can achieve a better detection performance than the existing ones in training-limited situations.

References

[1] HE Y, JIAN T, SU F, et al. Two adaptive detectors for range-spread targets in non-Gaussian clutter. Science China Information Sciences, 2011, 54: 386–395.

[2] JIAN T, HE Y, SU F, et al. High resolution radar target adaptive detector and performance assessment. Journal of Systems Engineering and Electronics, 2011, 22(2): 212–218.

[3] CUI G L, KONG L J, YAND X B, et al. Distributed target detection with polarimetric MIMO radar in compound-Gaussian clutter. Digital Signal Processing, 2012, 22(3): 430–438.

[4] JIAN T, HE Y, SU F, et al. Robust detector for range-spread targets in non-Gaussian background. Journal of Systems Engineering and Electronics, 2012, 23(3): 355–363.

[5] GAO Y C, AUBRY A, DE M A. Adaptive target separation detection. IEEE Trans. on Aerospace and Electronic Systems, 2021, 57(1): 293-309.

[6] LIU J, LIU W J, TANG B, et al. Distributed target detection exploiting persymmetry in Gaussian clutter. IEEE Trans. on Signal Processing, 2019, 67(4): 1022–1033.

[7] LIU W J, GAO F, LUO Y W, et al. GLRT-based generalized direction detector in partially homogeneous environment. Science China Information Sciences, 2019, 62(10): 209–303.

[8] RAGHAVAN R S. A CFAR detector for mismatched eigenvalues of training sample covariance matrix. IEEE Trans. on Aerospace and Electronic Systems, 2019, 67(17): 4624–4635.

[9] LIU W J, LIU J, GAO Y C, et al. Multichannel signal detection in interference and noise when signal mismatch happens. Signal Processing, 2020, 166: 107268.

[10] RAGHAVAN R S. A generalized version of ACE and performance analysis. IEEE Trans. on Signal Processing, 2020, 68(4): 2574–2585.

[11] COLUCCIA A, RICCI G, BESSON O. Design of robust radar detectors through random perturbation of the target signature. IEEE Trans. on Signal Processing, 2019, 67(19): 5118–5129.

[12] LIU W J, LIU J, HAO C, et al. Multichannel adaptive signal detection: basic theory and literature review. Science China Information Sciences, 2021. DOI:10.1007/s11432-020-3211-8.

[13] CONTE E, DE MAIO A, RICCI G. GLRT-based adaptive detection algorithms for range-spread targets. IEEE Trans. on Signal Processing, 2001, 49: 1336–1348.

[14] LIU W J, XIE W C, WANG Y L. Adaptive detection based on orthogonal partition of the primary and secondary data. Journal of Systems Engineering and Electronics, 2014, 25(1): 34–42.

[15] LIU W J, WANG Y L, LIU J, et al. Performance analysis of adaptive detectors for point targets in subspace interference and Gaussian noise. IEEE Trans. on Aerospace and Electronic Systems, 2018, 54(1): 429–441.

[16] LIU W J, LIU J, LI H, et al. Multichannel signal detection based on Wald test in subspace interference and Gaussian

noise. IEEE Trans. on Aerospace and Electronic Systems, 2019, 55(3): 1370–1381.
[17] CIUONZO D, DE MAIO A, ORLANDO D. On the statistical invariance for adaptive radar detection in partially homogeneous disturbance plus structured interference. IEEE Trans. on Signal Processing, 2017, 65(5): 1222–1234.
[18] BANDIERA F, DE MAIO A, GRECO A S, et al. Adaptive radar detection of distributed targets in homogeneous and partially homogeneous noise plus subspace interference. IEEE Trans. on Signal Processing, 2007, 55(4): 1223–1237.
[19] LIU W J, LIU J, HUANG L, et al. Rao tests for distributed target detection in interference and noise. Signal Processing, 2015, 117: 333–342.
[20] GAO Y C, LIAO G S, and LIU W J. High-resolution radar detection in interference and nonhomogeneous noise. IEEE Signal Processing Letters, 2016, 23(10): 1359–1363.
[21] LIU J, LIU W J, LI H, et al. False alarm rate of the GLRT for subspace signals in subspace interference plus Gaussian noise. IEEE Trans. on Signal Processing, 2019, 67(11): 3058–3069.
[22] ADDABBO P, BESSON O, ORLANDO D, et al. Adaptive detection of coherent radar targets in the presence of noise jamming. IEEE Trans. on Aerospace and Electronic Systems, 2019, 67(24): 6498–6510.
[23] LIU J, LI J. Analytical performance of rank-one signal detection in subspace interference plus Gaussian noise. IEEE Trans. on Aerospace and Electronic Systems, 2020, 56(2): 1595–1601.
[24] TANG P Q, WANG Y L, LIU W J, et al. Adaptive subspace signal detection in a type of structure nonhomogeneity environment. Signal Processing, 2019, 173: 107600.
[25] NITZBERG R. Application of maximum likelihood estimation of persymmetric covariance matrices to adaptive processing. IEEE Trans. on Aerospace and Electronic Systems, 1980, AES-16: 124–127.
[26] PAILLOUX G, FORSTER P, OVARLEZ J P. Persymmetric adaptive radar detectors. IEEE Trans. on Aerospace and Electronic Systems, 2011, 47: 2376–2390.
[27] LIU J, CUI G L, LI H B, et al. On the performance of a persymmetric adaptive matched fifilter. IEEE Trans. on Aerospace and Electronic Systems, 2015, 51(4): 2605–2614.
[28] HAO C P, ORLANDO D, MA X C, et al. Persymmetric Rao and Wald tests for partially homogeneous environment. IEEE Signal Processing Letters, 2012, 19(9): 587–590.
[29] WANG Z Y, LI M, CHEN H M, et al. Persymmetric detectors of distributed targets in partially homogeneous disturbance. Signal Processing, 2016, 128: 382–388.
[30] GAO Y C, LIAO G S, ZHU S Q, et al. Persymmetric adaptive detectors in homogeneous and partially homogeneous environments. IEEE Trans. on Signal Processing, 2014, 62(2): 331–342.
[31] CIUONZO D, ORLANDO D, PALLOTTA L. On the maximal invariant statistic for adaptive radar detection in partially homogeneous disturbance with persymmetric covariance. IEEE Signal Processing Letters, 2016, 23(12): 1830–1834.
[32] GAO Y C, LIAO G S, ZHU S Q, et al. Generalised persymmetric parametric adaptive coherence estimator for multichannel adaptive signal detection. IET Radar Sonar Navigation, 2015, 9(5): 550–558.
[33] LIU J, LIU S, LIU W J, et al. Persymmetric adaptive detection of distributed targets in compound-Gaussian sea clutter with Gamma texture. Signal Processing, 2018, 152: 340–349.
[34] LIU J, ORLANDO D, ADDABBO P, et al. SINR distribution for the persymmetric SMI beamformer with steering vector mismatches. IEEE Trans. on Signal Processing, 2019, 67(5): 1382–1392.
[35] LIU J, LI J. Mismatched signal rejection performance of the persymmetric GLRT detector. IEEE Trans. on Signal Processing, 2019, 67(6): 1610–1619.
[36] GAO Y C, JI H, LIU W J. Persymmetric adaptive subspace detectors for range-spread targets. Digital Signal Processing, 2019, 89(4): 116–123.
[37] LIU J, LIU W J, HAO C P, et al. Persymmetric subspace detectors with multiple observations in homogeneous environments. IEEE Trans. on Aerospace and Electronic Systems, 2020, 56(4): 3276–3284.
[38] LIU J, LIU W J, TANG B, et al. Persymmetric adaptive detection in subspace interference plus Gaussian noise. Signal Processing, 2020, 167: 107316.
[39] LIU J, JIAN T, LIU W J. Persymmetric detection of subspace signals based on multiple observations in the presence of subspace interference. Signal Processing, 2021, 183: 107–115.
[40] LIU J , CHEN J , LI J. Persymmetric adaptive detection of distributed targets with unknown steering vectors. IEEE Trans. on Signal Processing, 2020, 68(4): 4123−4134.
[41] LIU J, JIAN T, LIU W J. Persymmetric adaptive detection with improved robustness to steering vector mismatches. Signal Processing, 2020, 176: 107669.
[42] LIU J, SUN S. One-step persymmetric GLRT for subspace signals. IEEE Trans. on Signal Processing, 2019, 67(14): 3639–3648.
[43] LIU J, LIU W J, GAO Y C, et al. Persymmetric adaptive detection of subspace signals: algorithms and performance analysis. IEEE Trans. on Signal Processing, 2018, 66(23): 6124–6136.
[44] LIU J, LIU W J, LIU H W, et al. Average SINR calculation of a persymmetric sample matrix inversion beamformer. IEEE Trans. on Signal Processing, 2016, 64(8): 2135–2145.
[45] HAO C P, ORLANDO D, MA X C. Persymmetric detectors with enhanced rejection capabilities. IET Radar, Sonar & Navigation, 2014, 8(5): 557–563.
[46] MAO L L, GAO Y C, YAN S F, et al. Persymmetric subspace detection in structured interference and non-homogeneous disturbance. IEEE Signal Processing Letters, 2019, 26(6): 928–932.
[47] KAY S, and ZHU Z H. The complex parameter Rao test. IEEE Trans. on Signal Processing, 2016, 64(24): 6580–6588.
[48] LIU W J, WANG Y L, XIE W C. Fisher information matrix, Rao test, and Wald test for complex-valued signals and their applications. Signal Processing, 2014, 94: 1–5.
[49] SOHN K J, LI H B, HIMED B. Parametric GLRT for multichannel adaptive signal detection. IEEE Trans. on Signal Processing, 2007, 55(11): 5351–5360.

Biographies

GAO Yongchan was born in 1979. She received her Ph.D. degree in electronic engineering from Xidian University in 2015. From February 2016 to January 2017, she was a postdoctoral research associate with the Department of Electrical and Computer Engineering, Stevens Institute of Technology, Hoboken, NJ, USA. In March 2017, she joined the Electronic Engineering Department, Xidian University, where she is currently an associate professor. Her research interests include adaptive target detection, multistatic radar, passive sensing, and waveform design and diversity.
E-mail: ycgao@xidian.edu.cn

MAO Linlin was born in 1991. She received her Ph.D. degree in signal and information processing from Northwestern Polytechnical University, China in 2018. She is currently a research associate in the Institute of Acoustics, Chinese Academy of Sciences, since 2018. Her research interests include adaptive target detection, array signal processing, and multi-sensor networks.
E-mail: maoll@mail.ioa.ac.cn

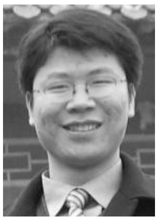

ZHU Shengqi was born in 1984. He received his Ph.D. degree in electrical engineering from Xidian University in 2010. In 2010 he joined Xidian University as a full assistant professor in the National Laboratory of Radar Signal Processing where he became an associate professor in 2012. His research interests include space-time adaptive processing, SAR ground moving target indication, and sparse signal processing.
E-mail: sqzhu@xidian.edu.cn

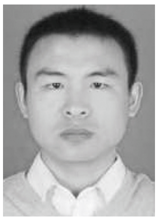

ZUO Lei was born in 1984. He received his Ph.D. degree from Xidian University in 2014. He is currently an associate professor in the National Laboratory of Radar Signal Processing, Xidian University. His current research interests include target detection, time-frequency analysis and synthesis, and time-frequency rate analysis.
E-mail: lzuo@mail.xidian.edu.cn